frontiers in Materials

ORIGINAL RESEARCH
published: 30 July 2021
doi: 10.3389/fmats.2021.710431

Microstructure and Oxidation Behavior of NiCoCrAlY Coating With Different Sm_2O_3 Concentration on TiAl Alloy

X. Gong[1,2], R. R. Chen[2], Y. Wang[2], Y. Q. Su[2], J. J. Guo[2] and H. Z. Fu[2]*

[1]College of Aerospace Engineering, Shenyang Aerospace University, Shenyang, China, [2]Department of Materials Science and Engineering, Harbin Institute of Technology, Harbin, China

In order to improve the oxidation resistance of TiAl alloys, NiCoCrAlY coatings with different amounts of Sm_2O_3 were prepared by laser cladding on TiAl alloys. The microstructure and oxidation behavior of the coatings were investigated by isothermal oxidation tests at 900°C. The results indicated that the grains of the coatings were refined by Sm_2O_3. The fine grain reduced the crack sensitivity of the doped coatings and promoted the transformation of θ-Al_2O_3 to α-Al_2O_3. Therefore, the internal oxidation of the coatings and the growth rate of the oxide films were reduced. The segregation of Sm at grain boundary inhibited the outward diffusion of Ti, thus reducing the excessive oxidation of Ti. In addition, the oxidation mechanism of the coating was changed from simultaneous diffusion of Al and O to predominant inward diffusion of O. The oxidation resistance of the doped coatings was significantly improved. However, excessive Sm_2O_3 is detrimental to the improvement of the oxidation resistance. The oxidation resistance of 3 wt% Sm_2O_3 is the best.

Keywords: NiCoCrAlY, rare earth, TiAl alloy, oxidation, laser cladding

Edited by:
Hao Zhang,
Jiangxi Science and Technology Normal University, China

Reviewed by:
Weiwei Sang,
Henan University of Engineering, China
Liang Wang,
Shanghai Institute of Ceramics (CAS), China

****Correspondence:***
R. R. Chen
chenruirun@163.com

Specialty section:
This article was submitted to Polymeric and Composite Materials, a section of the journal Frontiers in Materials

Received: *16 May 2021*
Accepted: *30 June 2021*
Published: *30 July 2021*

Citation:
Gong X, Chen RR, Wang Y, Su YQ, Guo J J and Fu HZ (2021) Microstructure and Oxidation Behavior of NiCoCrAlY Coating With Different Sm_2O_3 Concentration on TiAl Alloy. Front. Mater. 8:710431. doi: 10.3389/fmats.2021.710431

INTRODUCTION

TiAl-based alloys are promising structural materials due to their low density, high specific strength, and good creep resistance. They are considered a replacement for heavy nickel superalloys (Yamaguchi et al., 2000; Djanarthany et al., 2001; Wu, 2006; Perrut et al., 2018). However, the application of TiAl alloys is limited by their insufficient oxidation resistance at high temperatures (above 800°C). Alloying elements have been proposed to improve oxidation resistance at high temperatures, for example, V, Cr, Mn, and Nb (Lee, 2005; Vojtech et al., 2011; Raji et al., 2020). Excessive alloying may degrade the mechanical properties of the alloys. Furthermore, the mixture of TiO_2 and Al_2O_3 is formed on the surface of TiAl alloys in the oxidizing environment. The mixed oxide scale is non-protective. The porous TiO_2 deteriorates the adhesion between the oxide film and the alloy (Kim et al., 2014; Song et al., 2014). In this case, surface coating is an effective approach to improve the oxidation resistance of TiAl alloys.

MCrAlY (M = Ni, Co, or NiCo) is a typical class of oxidation-resistant coatings. It has been widely applied in turbine blades and other components for high-temperature applications. MCrAlY coatings are usually used as a single overlayer or a bond coating of thermal barrier coatings (TBC) (Liu et al., 2015; Shen et al., 2015; Zakeri et al., 2020; Hu et al., 2021). The concentration of Al in MCrAlY coating is very important because it directly affects the formation of the protective Al_2O_3

film. However, the inward diffusion of alloying elements will lead to a depletion of Al and instability of alloy during long-term service. In addition, the outward diffusion of alloying elements in the substrate can reduce the adhesion of the oxide scale. The oxidation resistance and lifetime of MCrAlY coatings are limited by severe elemental interdiffusion. Efforts have been made to modify the MCrAlY coatings in recent years. Previous studies (Haynes et al., 2007; Liu et al., 2008; Xu et al., 2009; Liang et al., 2011; Galiullin et al., 2018; Ghadami et al., 2020) have found that the oxidation resistance of MCrAlY coatings was improved by Re, Si, Pt, and Co. Compared with other elements, rare earth (RE) elements exhibit a more prominent effect due to their reactive element effects (REEs). Li et al. (2013a) and Pint et al. (2010) have found that the addition of REs can enhance the adhesion of the oxide scale on the alloy, thereby reducing the oxidation rate. (Li et al., 2006; Gil et al., 2009) have reported that the addition of Y_2O_3 inhibited the growth of columnar grains and promoted the formation of equiaxed grains. They also have found that the Y-distribution has a great influence on the morphology, growth rate, and mechanical stability of the Al_2O_3 scale, directly affecting the service life of the MCrAlY coatings. (Li et al., 2013b; Guo et al., 2014) have investigated the effect of REs on the oxidation resistance of NiAl alloys. The results have shown that Dy, La, Gd, Nd, Sc, Yb, and Sm contributed to improving oxide scale adhesion. Yb and Sc also reduced the oxidation rate of NiAl alloys. However, a large number of studies have been focused on the effect of Ce, La, and Y on the oxidation behavior of the coatings. Few studies have been done on the other rare earth elements, especially for Sm. Although Guo et al. have investigated the effect of Sm on the oxidation resistance of NiAl alloy, the effect of NiCoCrAlY coating has not been explored until now. Therefore, it is necessary to investigate the Sm-doped NiCoCrAlY coating systematically. Moreover, the effect of different concentrations of Sm on the oxidation behavior of NiCoCrAlY coating on TiAl alloy should be investigated.

In this work, laser cladding technique was used to prepare the NiCoCrAlY-xSm_2O_3 coatings on Ti44Al6Nb1Cr alloys (x = 0, 1, 3, 5 wt%). The characteristics of laser cladding are concentrated heat and small heat affected zone (Wang et al., 2020; Wang et al., 2021). It is an ideal method for the joining of dissimilar materials. The effects of Sm_2O_3 content on the microstructure, morphologies, phase composition, and oxidation behavior of NiCoCrAlY coating were systematically investigated by isothermal oxidation tests at 900°C.

EXPERIMENTAL PROCEDURE

Substrate Material and Coating Preparation

The Ti-44Al-6Nb-1Cr (at%) alloys used in this work were produced by vacuum consumable melting under an Ar atmosphere. Rectangular samples with a dimension of 30 mm × 15 mm × 2 mm were used as substrates. In order to produce a smooth surface without contaminants, the specimens were progressively polished with SiC papers down to 800-grit, peened with 200-grid brown fused alumina, ultrasonically washed with acetone, and finally dried in air. The NiCoCrAlY powders were provided by the Institute of Metal Research, Chinese Academy of Sciences. The chemical composition of the powder is shown in **Table.1**. Sm_2O_3 was added to the NiCoCrAlY powders with 1, 3, and 5 wt %, respectively. The NiCoCrAlY and Sm_2O_3 powders were mechanically milled at a rate of 260 rpm for 3 h in an Ar atmosphere. Stainless steel balls with diameters of Φ6 mm and Φ10 mm were used. The powder-to-ball mass ratio was set to 1:18. All the coatings were prepared by laser cladding. The mixed powder was placed on the Ti44A6lNb1Cr alloy with a thickness of 1 mm. An Nd: YAG laser system (FL-Dlight-1500) was used for the cladding. The process parameters used in the experiment have been optimized. The laser power is 700 W. The laser scanning speed is 300 mm/min. The spot dimension is 3 mm× 1 mm, and the overlapping rate is 30%. A shielding of Ar gas was used to protect the melting region from oxidization.

TABLE 1 | Chemical compositions of the powder (wt%).

Material	Ni	Co	Cr	Al	Y	Fe	Si	Ti	C
NiCoCrAlY	Bal	19.7	20.03	11.3	0.55	0.069	0.04	0.01	0.006

Oxidation Test

Isothermal oxidation tests of the NiCoCrAlY-xSm_2O_3 coatings were conducted. Some specimens with NiCoCrAlY coatings were used as the benchmark for comparison. The isothermal oxidation tests were performed in a muffle furnace at 900°C for 100 h. The specimen was put into a corundum crucible during oxidation. The mass gain was measured after prescribed time intervals by an electronic balance (0.1 mg precision). Two parallel specimens for each composition were used in the test.

The microstructure, morphology, and chemical composition of the coatings were observed by a Quanta 200FEG scanning electron microscope (SEM) equipped with energy dispersive spectroscopy (EDS). The phases of the coatings and oxide scales were identified by X-ray diffraction analysis (XRD, Model D/max-B, Japan) with Cu K_α radiation. The specimens were scanned in a 2θ range of 10-90° with a speed of 4°/min.

RESULTS AND DISCUSSION

As-Deposited Coating Characteristics

The surface morphologies of the as-deposited NiCoCrAlY coatings with 0, 1, 3, and 5 wt % Sm_2O_3 are shown in **Figure 1**. The surface of NiCoCrAlY coating is uneven. The surfaces of NiCoCrAlY coatings with Sm_2O_3 are flat, indicating that Sm_2O_3 has a great effect on the morphology of the surface of the NiCoCrAlY coating. (Gil et al., 2006) have found that the morphology of the oxide film was greatly affected by the surface roughness of the coating. The oxide film on the rough surface was inhomogeneous, and the distribution of Y and Al is uneven. The reduction of Y at the convex surfaces may lead to the spallation of the oxide film. The flat surface is conducive to enhancing the adhesion of the oxide film. The friction performance and fatigue resistance of the material were also greatly affected by surface

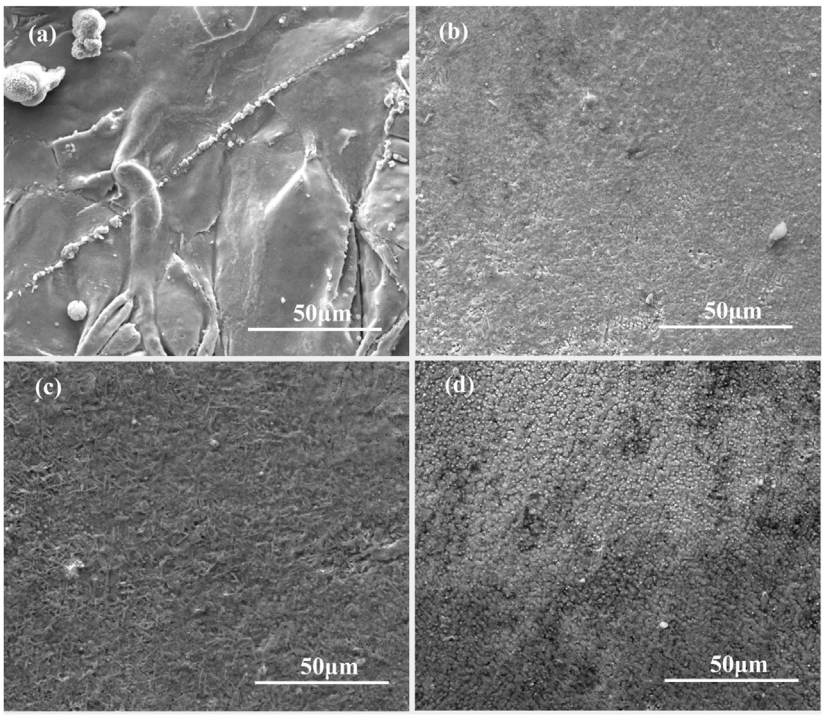

FIGURE 1 | Surface morphologies of the as-deposited coatings containing **(A)** 0 wt% Sm_2O_3; **(B)** 1 wt% Sm_2O_3; **(C)** 3 wt% Sm_2O_3; **(D)** 5 wt% Sm_2O_3.

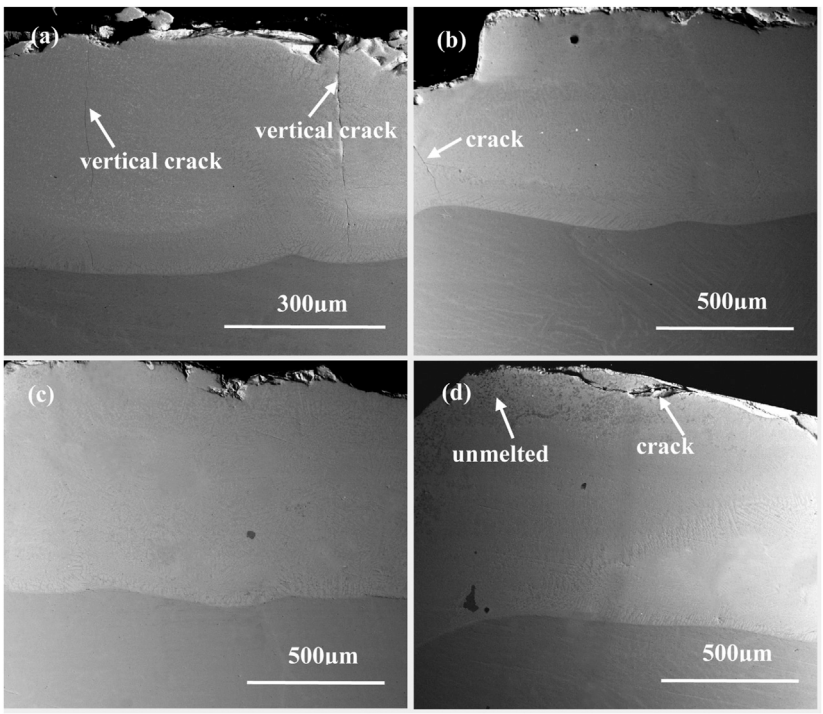

FIGURE 2 | Cross-sectional morphologies of the as-deposited coatings containing **(A)** 0 wt% Sm_2O_3; **(B)** 1 wt% Sm_2O_3; **(C)** 3 wt% Sm_2O_3; **(D)** 5 wt% Sm_2O_3.

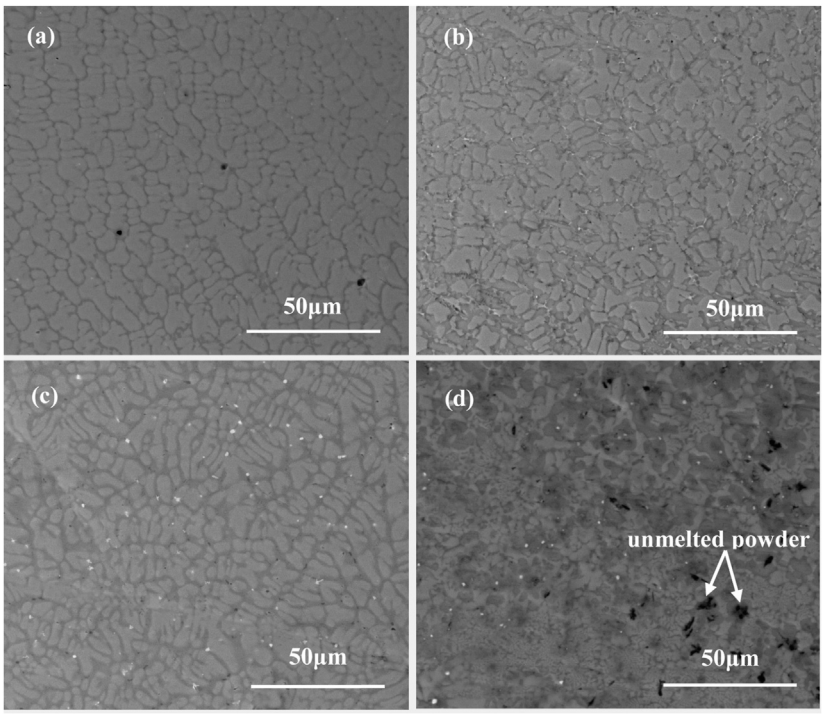

FIGURE 3 | Cross-sectional morphologies of the as-deposited coatings near the interface: **(A)** 0 wt% Sm_2O_3; **(B)** 1 wt% Sm_2O_3; **(C)** 3 wt% Sm_2O_3; **(D)** 5 wt% Sm_2O_3.

roughness. The smooth surface is helpful to reduce the wear and fatigue of the coating during service. (Sun et al., 2010) have studied the laser absorption by metallic materials. The laser absorptivity is as follows (Djanarthany et al., 2001):

$$A_D = 1 - R_D = \left(\frac{2\omega}{\pi\sigma_0}\right)^{1/2} \left[\left(1+\omega^2\tau^2\right)^{1/2} - \omega\tau\right]^{1/2}, \qquad (1)$$

where A_D is the laser absorptivity, ω is the frequency of lightwave, τ is the relaxation time, and σ_0 is the conductivity. According to **Eq.1**, the laser absorptivity of coating is related to laser wavelength and metallic conductivity. In this work, since the same process parameters are used to prepare the coating, the laser wavelength is the same. Therefore, the laser absorptivity of the coatings is only inversely proportional to conductivity. The conductivity of ceramic oxide is lower than that of metal. The addition of Sm_2O_3 reduced the conductivity and enhanced the laser absorptivity of the NiCoCrAlY coating. The high laser absorptivity increased the fluidity of the liquid metal, thereby improving the flatness of the coating.

Figure 2 displays the cross-section morphologies of the as-deposited NiCoCrAlY coatings with different content of Sm_2O_3. All the coatings were well bonded to the TiAl alloys. The wavy morphologies of the interface suggest that the bonding between the coatings and substrates is metallurgical, which is beneficial to enhance the adhesion of the coating. For the NiCoCrAlY coating, two vertical cracks are extended from the surface to the interface. The vertical cracks have a great influence on oxidation resistance. It is expected that oxygen can diffuse rapidly inward to the coating/metal interface through cracks during the oxidation process. Therefore, the internal oxidation of the metal substrate will be induced by the vertical cracks. The formation of the oxides will reduce the adhesion strength between the coating and substrate. However, the addition of Sm_2O_3 changed the formation mechanism of the crack. It can be seen that there are few cracks in the 1 wt% Sm_2O_3 coating and no cracks in the 3wt% Sm_2O_3 coatings. Some transverse cracks are observed near the surface in the 5wt% Sm_2O_3 coating. It can be found that Sm_2O_3 has a great effect on the formation of cracks.

In order to analyze the effect of Sm_2O_3 on the crack sensitivity of NiCoCrAlY coating, the microstructure of the doped coatings near the surface is investigated. The cross-sectional morphologies of the as-deposited coatings near the surface are shown in **Figure 3**. As can be seen in **Figure 3**, the addition of Sm_2O_3 refined the microstructure of the coatings. Moreover, the grain size of the coating decreased with the increase of Sm_2O_3. For laser cladding processing, the material will undergo rapid heating and cooling. Therefore, heterogeneous nucleation often occurs in liquid metal. The new phase cores are usually formed on unmelted particles in the molten pool. The nucleation surface energy can be reduced by using this nucleation way. In this work, unmelted Sm_2O_3 particles play the role of heterogeneous nucleation sites. The increase of the heterogeneous nucleation sites decreased the nucleation surface energy, which promoted the nucleation of liquid metal. Due to the REEs, rare earth elements will reduce the surface tension of the coating.

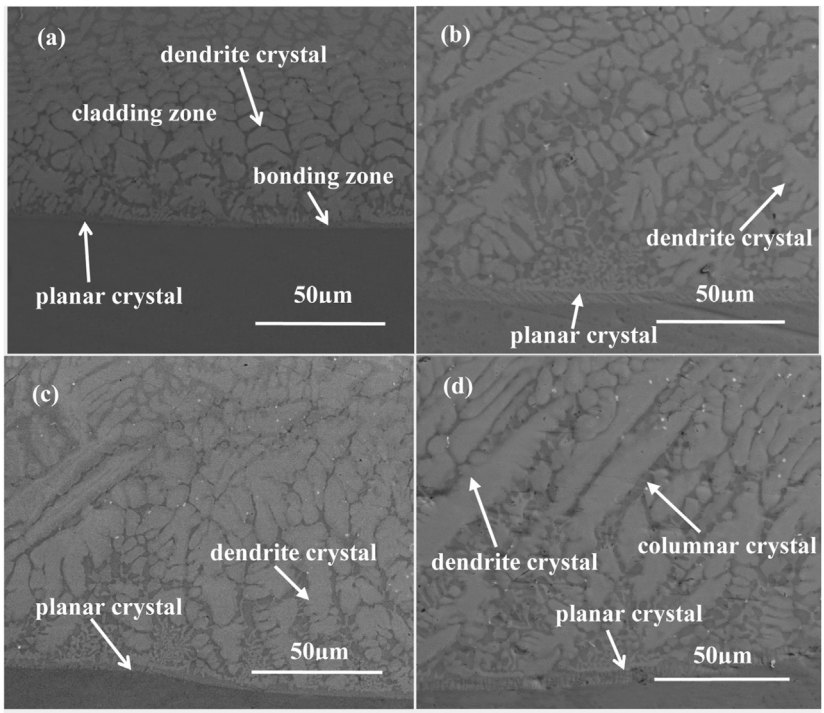

FIGURE 4 | Cross-sectional morphologies of the as-deposited coatings near the interface: **(A)** 0 wt% Sm_2O_3; **(B)** 1 wt% Sm_2O_3; **(C)** 3 wt% Sm_2O_3; **(D)** 5 wt% Sm_2O_3.

According to the Guggenheim equation (Kamalyan, 2010), the decrease of surface tension results in the decrease of critical nucleation work. In addition, rare earth elements tend to segregate to grain boundaries during solidification. This is because the atomic radius of rare earth atoms is large. So, the distortion energy of rare earth elements is small at the crystal boundary. The segregation of rare earth elements hinders the movement of the grain boundary. As a result, the grain sizes of the NiCoCrAlY-*x*Sm_2O_3 coatings are reduced. The refinement of microstructure is beneficial to reduce the probability and degree of stress concentration in the coating. Meanwhile, it hinders the propagation of cracks in grains and grain boundaries. The small grain causes the deformation to be distributed in more grains so that the difference of strain degree within and near grain boundaries is reduced. In other words, the deformation degree becomes uniform. The degree of stress concentration in the coating is reduced. Therefore, the probability and degree of cracking in the coating decrease. In the 5 wt% Sm_2O_3 coating, a large number of Sm_2O_3 aggregates at the surface zone, which reduces the fluidity of liquid alloy in the molten pool. The slags cannot float before solidification, thereby increasing the crack sensitivity of the coating. Therefore, some transverse cracks were formed at the aggregation of unmelted Sm_2O_3 particles. However, the direction and depth of the cracks were changed by the unmelted particles. Compared with the vertical crack, the transverse crack only induces the internal oxidation of the surface zone in the coating. It can be concluded that moderate Sm_2O_3 can reduce the tendency of cracking by improving the fluidity of the liquid metal during cladding.

The cross-sectional morphologies of the as-deposited coatings near the interface are shown in **Figure 4**. According to the characteristics of the solidification structure, the zone near the interface can be further divided into a cladding zone and a bonding zone. It can be seen that the bonding zones of all the coatings are composed of planar crystals. Planar crystals are formed when the ratio between the temperature gradient (G) and the solidification speed (v) is high. With the increase of Sm_2O_3, the width of the bonding zone increased. This is because NiCoCrAlY-Sm_2O_3 coatings absorbed more laser energy and elevated the temperature of the molten pool. Therefore, the temperature gradient at the liquid-solid interface increased. In the cladding zone of the NiCoCrAlY coating, the dendritic structure can be observed. The growth direction of the dendritic crystal is perpendicular to the interface between the coating and alloy. After adding Sm_2O_3, dendritic crystal decreases and columnar crystal increases. The melting of dendritic arms is caused by the enrichment of rare earth elements. Due to the large atomic radius, it is easy to enrich Sm^{3+} in the interdendritic and the front edge of the liquid-solid interface during the deposition process. The enrichment of the Sm^{3+} promoted the fusing of the dendrite crystal and prevented the growth of the columnar crystals along the vertical direction. The reduction of dendrite crystal is beneficial to improve the mechanical properties of the as-deposited coating.

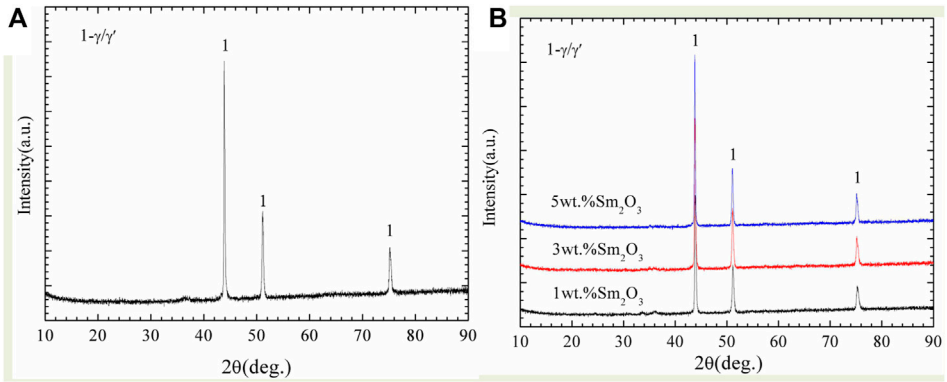

FIGURE 5 | XRD patterns of the as-deposited **(A)** NiCoCrAlY coating and **(B)** NiCoCrAlY-xSm_2O_3 coatings.

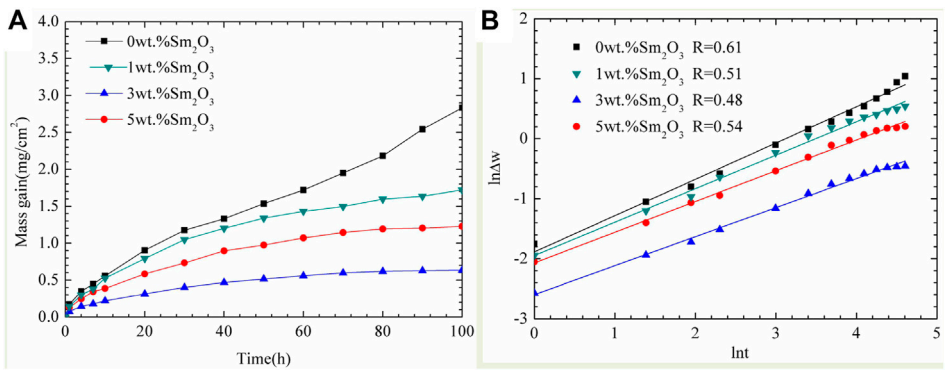

FIGURE 6 | (A) Mass gain vs. time of the NiCoCrAlY-xSm_2O_3 coatings; **(B)** plots of lnΔw vs. lnt for the oxidation behavior fitted from the curves in **(A)**.

TABLE 2 | Oxidation rate constants (k_p) of the NiCoCrAlY-xSm_2O_3.

Material	Oxidation time(h)	*N*	Oxidation rate constant ($mg^n \cdot cm^{-2n} \cdot s^{-1}$)
0 wt% Sm_2O_3	0–100	1.63	1.23×10^{-5}
1 wt% Sm_2O_3	0–100	1.85	8.46×10^{-6}
3 wt% Sm_2O_3	0–100	2.08	1.29×10^{-6}
5 wt% Sm_2O_3	0–100	1.96	4.88×10^{-6}

Figure 5 displays the phase compositions of the as-deposited NiCoCrAlY-xSm_2O_3 coatings. The phases in the NiCoCrAlY and NiCoCrAlY-xSm_2O_3 coatings are mainly composed of γ and γ'. Because the addition of Sm_2O_3 is less, the peak of Sm_2O_3 can not be detected.

Oxidation Kinetics

Figure 6 illustrates the difference in isothermal oxidation resistance at 900°C between the NiCoCrAlY and NiCoCrAlY-xSm_2O_3 coatings. As shown in **Figure 6A**, the mass gain of the NiCoCrAlY coatings during the oxidation is reduced by the addition of Sm_2O_3. Our previous research has found that NiCoCrAlY coating helps improve the isothermal oxidation resistance of Ti44Al6Nb1Cr alloy (Gong et al., 2018). It is clear that the addition of Sm_2O_3 further enhanced the oxidation resistance of NiCoCrAlY coating. The mass gain of the NiCoCrAlY coating has reached 2.83 mg/cm^2 after oxidation for 100 h. A sharp increase of the mass gain occurs from 60 to 100 h. The mass gain of the doped coatings depends on the contents of Sm_2O_3 in the coatings. The mass gain of 3 wt% Sm_2O_3 coating is the lowest, indicating that it possesses the best oxidation resistance. The oxidation constant k_p is calculated as follows:

$$\Delta w^n = k_p t, \tag{2}$$

where Δw represents the weight gain per unit area (mg/cm^2), n is the power exponent, k_p is the oxidation rate constant ($mg^n \cdot cm^{-2n} \cdot h^{-1}$), and t is the oxidation time (h). The values of n and k_p were tested by Origin software based on **Eq. 2**. In **Figure 6B**, the log of mass gain was plotted versus the log of oxidation time to investigate the oxide scale growth rate. It can be seen that NiCoCrAlY-xSm_2O_3 coatings follow a parabolic law during 100 h oxidation. However, the NiCoCrAlY coating follows a parabolic law in the first 50 h. Linear growth can be seen from

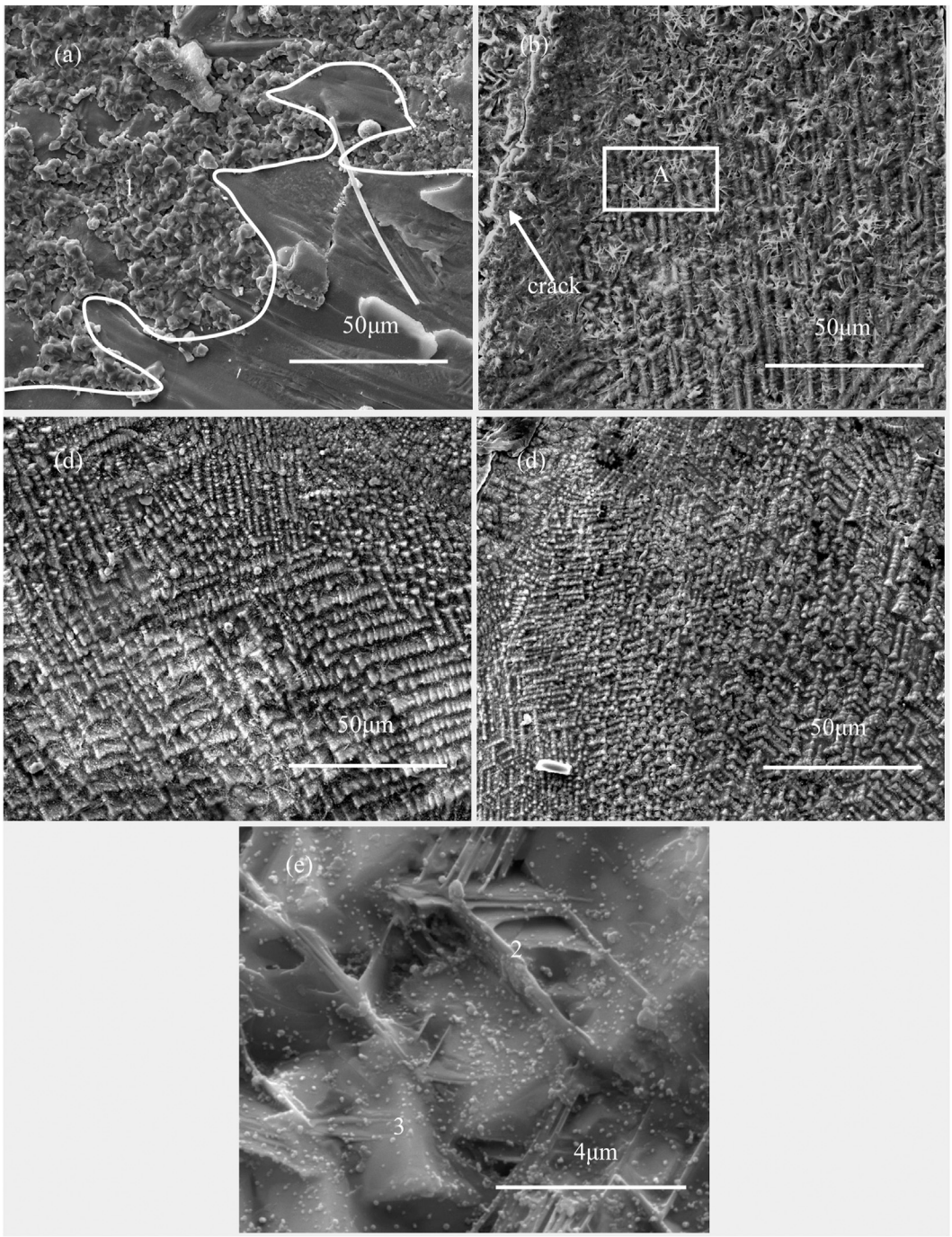

FIGURE 7 | Surface morphologies of the coatings containing **(A)** 0 wt% Sm_2O_3; **(B)** 1 wt% Sm_2O_3; **(C)** 3 wt% Sm_2O_3; **(D)** 5 wt% Sm_2O_3. **(E)** The magnified figure of zone A after oxidation at 900°C for 100 h.

TABLE 3 | Chemical composition of the oxides on the NiCoCrAlY-xSm_2O_3 coatings (at%).

Point	Ni	Co	Cr	Al	Y	Sm	O	Ti	Phase
1	6.53	3.36	3.69	17.45	3.17	—	35.29	33.68	TiO_2+Al_2O_3
2	0.40	0.20	0.91	48.5	2.36	6.68	39.0	1.58	θ-Al_2O_3
3	3.48	0.08	1.54	31.0	5.77	15.4	40.9	1.83	α-Al_2O_3

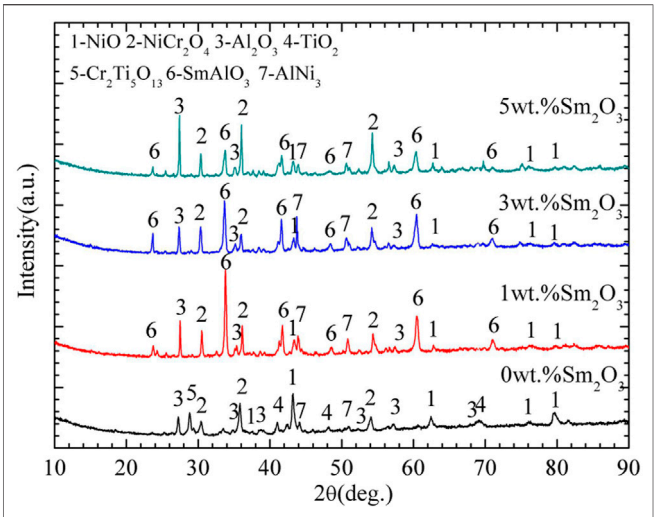

FIGURE 8 | XRD patterns of the NiCoCrAlY-xSm_2O_3 coatings after oxidation at 900°C for 100 h.

60 to 100 h. The linear growth indicates a high oxidation rate. The oxidation rate constants are listed in **Table.2**. The value of k_p for NiCoCrAlY coating is 1.23×10^{-5} mg^2 cm^{-4} s^{-1}. For the doped coating, the oxidation rate constant of 3 wt% Sm_2O_3 coating is the lowest, whereas that of 1 wt% Sm_2O_3 coating is the highest, indicates that the oxidation resistance of 3 wt% Sm_2O_3 coating is the best. However, the value of k_p for 1 wt% Sm_2O_3 coating is 8.46×10^{-6} mg^2 cm^{-4} s^{-1}, which is lower than that for NiCoCrAlY coating. By comparing the values of k_p, it can be found that the oxidation rate of NiCoCrAlY coating has been reduced by order of magnitude by the addition of Sm_2O_3. In other words, the addition of Sm_2O_3 can improve the oxidation resistance of NiCoCrAlY coating. However, the oxidation resistance of the doped coating is not proportional to the content of rare earth elements. Excessive RE leads to the agglomeration of the cladding powders and reduces the uniformity of particle distribution. The high oxidation rate of 5 wt% Sm_2O_3 coating may be attributed to the transverse cracks in the surface zone. The transverse cracks will induce severe internal oxidation, which is detrimental to the oxidation resistance.

Oxidation Behavior

Figure 7 shows the surface morphologies of the NiCoCrAlY-xSm_2O_3 coatings after oxidation at 900°C for 100 h. In **Figure 7A**, the spalling of oxide film on the surface of NiCoCrAlY coating is observed, which indicates that the adhesion of the oxide scale is poor. According to EDS results, the oxides on NiCoCrAlY coating are composed of Al_2O_3 and TiO_2. TiO_2 is a non-protective oxide due to its high growth rate. The large amount of TiO_2 and incomplete oxide film is one of the main reasons for the poor oxidation resistance of NiCoCrAlY coating. For the doped coatings, the morphologies of oxide films changed obviously. **Figure 7E** is the magnified figure of zone A in **Figure 7B**. As shown in the figure, the oxide film on the 1 wt% Sm_2O_3 coating is composed of granular oxides and needle oxides. According to the EDS and XRD results, these oxides are α-Al_2O_3 and θ-Al_2O_3, respectively. The refinement effect of Sm_2O_3 promoted the

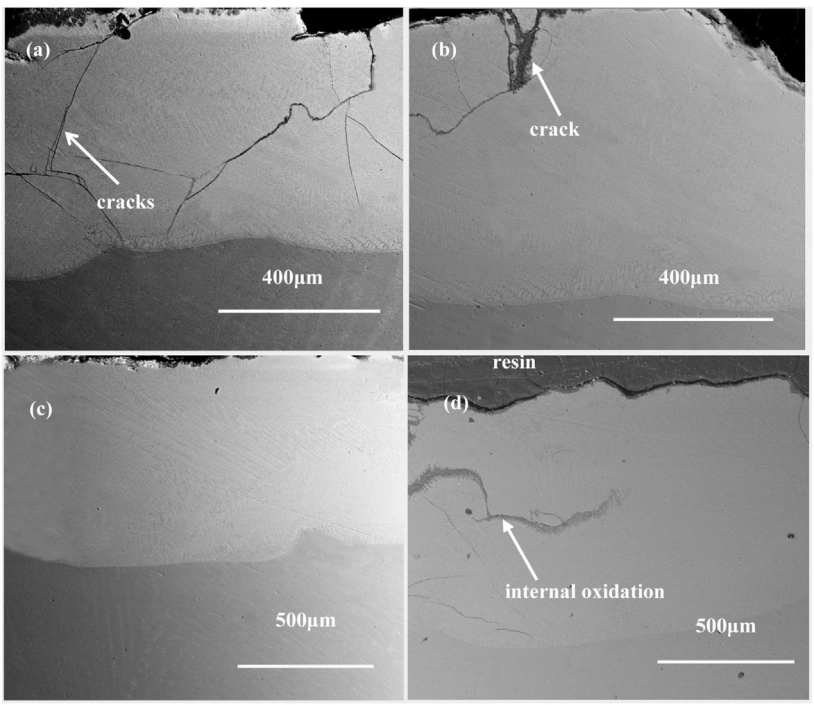

FIGURE 9 | Cross-sectional morphologies of the cotaings containing **(A)** 0 wt% Sm_2O_3; **(B)** 1 wt% Sm_2O_3; **(C)** 3 wt% Sm_2O_3; **(D)** 5 wt% Sm_2O_3 after oxidation at 900°C for 100 h.

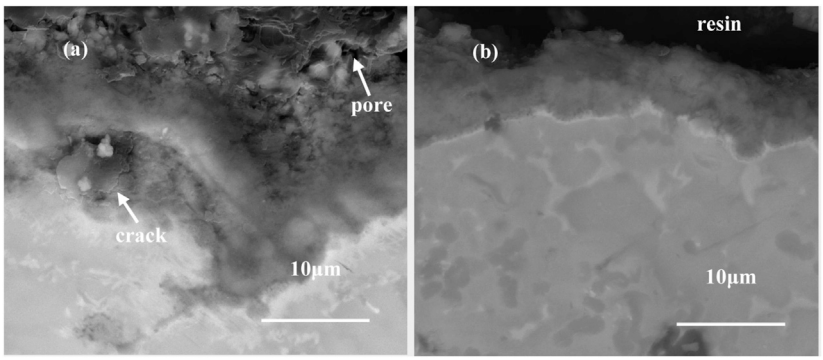

FIGURE 10 | Cross-sectional morphologies of the oxide films on the coatings containing **(A)** 0 wt% Sm_2O_3 and **(B)** 3 wt% Sm_2O_3 after oxidation at 900°C for 100 h.

selective oxidation of the Al element. With the increase of Sm_2O_3 content, the amount of θ-Al_2O_3 decreases. When the content of Sm_2O_3 reaches 3 wt%, the oxide film is mainly composed of α-Al_2O_3, indicating that Sm_2O_3 promoted the transition from θ-Al_2O_3 to α-Al_2O_3. According to **Table.3**, the content of Sm in the oxides on 5 wt% Sm_2O_3 coating is up to 15.4 at%. The growth of α-Al_2O_3 mainly depends on the diffusion of oxygen along the grains. Therefore, the structure of α-Al_2O_3 is denser than that of θ-Al_2O_3. The rapid transition of θ-Al_2O_3 to α-Al_2O_3 significantly reduces the growth rate of oxide film, thereby improving the oxidation resistance. In general, the transition of θ-Al_2O_3 to α-Al_2O_3 will induce the volume change of oxides, thereby increasing the stress in the oxide film. Although the transformation rate of Al_2O_3 is fast, the oxide film on the 3 wt % Sm_2O_3 and 5 wt% Sm_2O_3 coatings did not crack. This is because the addition of Sm_2O_3 refined the grain size of the oxides. With the increase of Sm_2O_3 content, the grain size of oxides decreases. The fine grain size can promote the release of internal stress through grain boundary slip. Therefore, the complete oxide films are formed on the 3 wt% Sm_2O_3 and 5 wt% Sm_2O_3 coatings, which is beneficial for improving the oxidation resistance of the coatings.

The phase compositions of the oxide scales on the coatings after oxidation at 900°C for 100 h are detected by XRD analysis, and the results are shown in **Figure 8**. The oxide scale of the undoped coating consisted of NiO, Al_2O_3, $NiCr_2O_4$, $Cr_2Ti_5O_{13}$, and little TiO_2. The formation of $Cr_2Ti_5O_{13}$ and TiO_2 is caused by the outward diffusion of Ti atoms. The formation of the two phases not only consumes Ti in the substrate but also consumes Cr in the coating. It is not conducive to oxidation resistance and mechanism properties. For the doped coatings, no Ti-oxides were detected. This is because the segregation of unmelted particles and rare earth elements at grain boundary can hinder the outward diffusion of Ti atoms. It is worth noting that $SmAlO_3$ is formed on the doped coatings. The reaction equations are as follows:

$$Al_2O_3 + Sm_2O_3 = 2SmAlO_3 \quad (3)$$

According to this reaction equation, the formation of $SmAlO_3$ is accompanied by the consumption of Al_2O_3, which is detrimental to the oxidation resistance of the coating.

The cross-sectional morphologies of the coatings after oxidation for 100 h were examined and the results are shown in **Figure 9**. In the un-doped coating, the vertical cracks extend from the surface to the interface. The penetrating cracks will accelerate the inward diffusion of oxygen and weaken the adhesion of the coating. Therefore, severe internal oxidation occurs in the un-doped coating. The addition of Sm_2O_3 reduces the number of cracks in the coating. Especially for the 3 wt% Sm_2O_3 coating, almost no cracks are observed. The results indicate that the addition of Sm_2O_3 can improve the growth resistance of cracks in laser cladding NiCoCrAlY coating. The refinement effect of Sm_2O_3 on coating microstructure is the reason for the good growth resistance of cracks. The refined grains reduced stress concentration in the coating. However, for the other coatings, a complete oxide film cannot be formed at the initial stage of oxidation due to the formation of cracks. The incomplete oxide film resulted in the increase of the oxidation rate.

The cross-sectional morphologies of the oxide scales after oxidation at 900°C for 100 h are shown in **Figure 10**. **Figure 10A** shows that the oxide film on the NiCoCrAlY coating is loose. Some pores and micro-cracks can be found in the oxide film, which are induced by the outward diffusion of metal cations. On the one hand, oxygen, Al^{3+} and Cr^{3+} diffused simultaneously through the oxide grain boundaries, which led to the formation of new oxides within the generated film. This growth behavior of oxides can result in large stresses within the oxide film. On the other hand, a large number of voids were formed at the interface due to the outward diffusion of Al^{3+} and Cr^{3+}. Under the action of the two factors, the spalling and plastic deformation of the oxide film occurred to release the growth stress in the oxide film. The oxide films become dense by the addition of Sm_2O_3. There is no pore and micro-crack in the oxide film. (Guo et al., 2011) have reported that the addition of Dy can restrain the growth of the oxide scale on NiAl alloy by decreasing the diffusion rate. The formation of the dense oxide film is related to grain boundary segregation and impurity purification of rare earth elements. The rare earth elements tend to segregate at grain boundaries during oxidation due to the atomic radius. In this work, the segregation of Sm inhibited the outward diffusion of Al^{3+} and Cr^{3+}. The oxidation mechanism of the coating was changed from

simultaneous diffusion of Al and O to predominant inward diffusion of O. The inhibition of the outward diffusion of metal cations reduced the formation of pores and oxidation rate. In addition, Sm hindered the aggregation of impurity elements at the interface, such as S, Cl, and P, which played a role in purifying the interface. As a result, a thin and dense oxide scale was formed on the surface of the doped coatings.

CONCLUSION

1) The width of plane crystal at the interface between the coating and TiAl alloy increased by the addition of Sm_2O_3. The enrichment of Sm between the dendrites and in front of liquid-solid boundaries led to the dendrites fusion, which promoted the growth of columnar crystals. At the near-surface region, the addition of Sm_2O_3 increased the nucleation particles in the molten pool, thereby refining the grains of the coating.
2) The addition of Sm_2O_3 enhanced the laser absorptivity of the NiCoCrAlY coating, thereby improving the fluidity of the liquid metal. Excessive doping reduced the fluidity of the liquid metal due to the segregation of Sm_2O_3 agglomerates.
3) The oxidation resistance of the NiCoCrAlY coating was improved effectively by the addition of Sm_2O_3. The refinement of grains is beneficial to improve oxidation resistance. However, excessive Sm_2O_3 addition is detrimental to the oxidation resistance because it resulted in internal oxidation. The coating doped with 3 wt% Sm_2O_3 was the optimized composition.
4) The propagation of the cracks in the doped coatings was suppressed. The crack sensitivity and residual stress of the coating were reduced by the addition of Sm_2O_3. The decrease of cracks is helpful to reduce the internal oxidation of the coatings.
5) The oxidation mechanism of the coating was changed by the addition of Sm_2O_3. The oxidation mechanism was changed from simultaneous diffusion of Al and O to predominant inward diffusion of O. A thin oxide scale was formed on the 3 wt% Sm_2O_3 coating, which is beneficial to enhance the adhesion of oxide scale.

DATA AVAILABILITY STATEMENT

The raw data supporting the conclusions of this article will be made available by the authors without undue reservation.

AUTHOR CONTRIBUTIONS

FH, CR, and WY designed experiments; GX carried out experiments; GX, SY, and GJ analyzed experimental results.

FUNDING

This work was supported by the National Natural Science Foundation of China (No. 52001217), Science and Technology Research of Liaoning Province Education Department (JYT19035), National Science and Technology Major Project (2017-Vl-0020-0093), and National Defense Key Laboratory Foundation of Shenyang Aerospace University (SHSYS 202005).

REFERENCES

Djanarthany, S., Viala, J.-C., and Bouix, J. (2001). An Overview of Monolithic Titanium Aluminides Based on Ti3Al and TiAl. *Mater. Chem. Phys.* 72, 301–319. doi:10.1016/s0254-0584(01)00328-5

Galiullin, T., Chyrkin, A., Pillai, R., Vassen, R., and Quadakkers, W. J. (2018). Effect of Alloying Elements in Ni-Base Substrate Material on Interdiffusion Processes in MCrAlY-Coated Systems. *Surf. Coat. Technol.* 350, 359–368. doi:10.1016/j.surfcoat.2018.07.020

Ghadami, F., Aghdam, A., and Ghadami, S. (2020). Microstructural Characteristics and Oxidation Behavior of the Modified MCrAlX Coatings: A Critical Review [J]. *Vacuum* 185, 109980. doi:10.1016/j.vacuum.2020.109980

Gil, A., Naumenko, D., Vassen, R., Toscano, J., Subanovic, M., Singheiser, L., et al. (2009). Y-Rich Oxide Distribution in Plasma Sprayed MCrAlY-Coatings Studied by SEM with a Cathodoluminescence Detector and Raman Spectroscopy. *Surf. Coat. Technol.* 204, 531–538. doi:10.1016/j.surfcoat.2009.08.034

Gil, A., Shemet, V., Vassen, R., Subanovic, M., Toscano, J., Naumenko, D., et al. (2006). Effect of Surface Condition on the Oxidation Behaviour of MCrAlY Coatings. *Surf. Coat. Technol.* 201, 3824–3828. doi:10.1016/j.surfcoat.2006.07.252

Gong, X., Chen, R. R., Yang, Y. H., Wang, Y., Ding, H. S., Guo, J. J., et al. (2018). Effect of Mo on Microstructure and Oxidation of NiCoCrAlY Coatings on High Nb Containing TiAl Alloys. *Appl. Surf. Sci.* 431, 81–92. doi:10.1016/j.apsusc.2017.07.026

Guo, H., Wang, D., Peng, H., Gong, S., and Xu, H. (2014). Effect of Sm, Gd, Yb, Sc and Nd as Reactive Elements on Oxidation Behaviour of β-NiAl at 1200°C. *Corrosion Sci.* 78, 369–377. doi:10.1016/j.corsci.2013.10.021

Guo, H., Zhang, T., Wang, S., and Gong, S. (2011). Effect of Dy on Oxide Scale Adhesion of NiAl Coatings at 1200°C. *Corrosion Sci.* 53, 2228–2232. doi:10.1016/j.corsci.2011.03.003

Haynes, J. A., Pint, B. A., Zhang, Y., and Wright, I. G. (2007). Comparison of the Cyclic Oxidation Behavior of β-NiAl, β-NiPtAl and γ-γ' NiPtAl Coatings on Various Superalloys. *Surf. Coat. Technol.* 202, 730–734. doi:10.1016/j.surfcoat.2007.06.039

Hu, S., Finklea, H., and Liu, X. (2021). A Review on Molten Sulfate Salts Induced Hot Corrosion. *J. Mater. Sci. Technol.* 90, 243–254. doi:10.1016/j.jmst.2021.03.013

Kamalyan, O. A. (2010). Guggenheim-Anderson-de Boer Isotherm Equation as Applied to Determining Texture Parameters of Sorbents with Compounds Grafted to Their Surfaces. *Colloid J.* 72, 286–288. doi:10.1134/s1061933x10020213

Kim, S.-W., Hong, J. K., Na, Y.-S., Yeom, J.-T., and Kim, S. E. (2014). Development of TiAl Alloys with Excellent Mechanical Properties and Oxidation Resistance. *Mater. Des. (1980-2015)* 54, 814–819. doi:10.1016/j.matdes.2013.08.083

Lee, D.-B. (2005). Effect of Cr, Nb, Mn, V, W and Si on High Temperature Oxidation of TiAl Alloys. *Met. Mater. Int.* 11, 141–147. doi:10.1007/bf03027458

Li, D., Guo, H., Peng, H., Gong, S., and Xu, H. (2013). Improved Alumina Scale Adhesion of Electron Beam Physical Vapor Deposited Dy/Hf-Doped β-NiAl Coatings. *Appl. Surf. Sci.* 283, 513–520. doi:10.1016/j.apsusc.2013.06.137

Li, D., Guo, H., Wang, D., Zhang, T., Gong, S., and Xu, H. (2013). Cyclic Oxidation of β-NiAl with Various Reactive Element Dopants at 1200°C. *Corrosion Sci.* 66, 125–135. doi:10.1016/j.corsci.2012.09.010

Li, M. X., He, Y. Z., and M Yuan, X. (2006). Effect of Nano-Y2o3 on Microstructure of Laser Cladding Cobalt-Based alloy Coatings. *Appl. Surf. Sci.* 252, 2882–2887. doi:10.1016/j.apsusc.2005.04.038

Liang, J. J., Wei, H., Zhu, Y. L., Sun, X. F., Jin, T., Hu, Z. Q., et al. (2011). Influence of Co Addition on Constituent Phases and Performance of a NiCrAlYRe alloy System. *Surf. Coat. Technol.* 205, 4968–4979. doi:10.1016/j.surfcoat.2011.04.084

Liu, X., Huang, L., Bao, Z. B., Sun, X. F., Guan, H. R., and Hu, Z. Q. (2008). Preparation and Cyclic Oxidation of Gradient NiCrAlYRe Coatings on Ni-Based Superalloys. *Surf. Coat. Technol.* 202, 4709–4713. doi:10.1016/j.surfcoat.2008.04.049

Liu, Y. Z., Hu, X. B., Zheng, S. J., Zhu, Y. L., Wei, H., and Ma, X. L. (2015). Microstructural Evolution of the Interface between NiCrAlY Coating and Superalloy during Isothermal Oxidation. *Mater. Des.* 80, 63–69. doi:10.1016/j.matdes.2015.05.014

Perrut, M., Caron, P., Thomas, M., and Couret, A. (2018). High Temperature Materials for Aerospace Applications: Ni-Based Superalloys and γ-TiAl Alloys. *Comptes Rendus Physique.* 19, 657–671. doi:10.1016/j.crhy.2018.10.002

Pint, B. A., Haynes, J. A., and Besmann, T. M. (2010). Effect of Hf and Y alloy Additions on Aluminide Coating Performance. *Surf. Coat. Technol.* 204, 3287–3293. doi:10.1016/j.surfcoat.2010.03.040

Raji, S. A., Popoola, A., Pityana, S. L., and Popoola, O. M. (2020). Characteristic Effects of Alloying Elements on β Solidifying Titanium Aluminides: A Review. *Heliyon* 6, e04463. doi:10.1016/j.heliyon.2020.e04463

Shen, M., Zhao, P., Gu, Y., Zhu, S., and Wang, F. (2015). High Vacuum Arc Ion Plating NiCrAlY Coatings: Microstructure and Oxidation Behavior. *Corrosion Sci.* 94, 294–304. doi:10.1016/j.corsci.2015.02.032

Song, Y., Xing, F. J., Dai, J. H., and Yang, R. (2014). First-principles Study of Influence of Ti Vacancy and Nb Dopant on the Bonding of TiAl/TiO2 Interface. *Intermetallics* 49, 1–6. doi:10.1016/j.intermet.2014.01.001

Sun, D., Tong, Y. G., and He, X. M. (2010). Study on Influence Factors of Laser Absorptivity in Laser Welding. *Hot. Work. Tech.* 39, 165–167. doi:10.14158/j.cnki.1001-3814.2010.19.046

Vojtech, D., Popela, T., Kubásek, J., Maixner, J., and Novák, P. (2011). Comparison of Nb- and Ta-Effectiveness for Improvement of the Cyclic Oxidation Resistance of TiAl-Based Intermetallics. *Intermetallics* 19, 493–501. doi:10.1016/j.intermet.2010.11.025

Wang, C., Li, J., Wang, T., Chai, L., Deng, C., Wang, Y., et al. (2021). Microstructure and Properties of Pure Titanium Coating on Ti-6Al-4V alloy by Laser Cladding. *Surf. Coat. Technol.* 416, 127137. doi:10.1016/j.surfcoat.2021.127137

Wang, Q.-Y., Pei, R., Liu, S., Wang, S.-L., Dong, L.-J., Zhou, L.-J., et al. (2020). Microstructure and Corrosion Behavior of Different Clad Zones in Multi-Track Ni-Based Laser-Clad Coating. *Surf. Coat. Technol.* 402, 126310. doi:10.1016/j.surfcoat.2020.126310

Wu, X. (2006). Review of alloy and Process Development of TiAl Alloys. *Intermetallics* 14, 1114–1122. doi:10.1016/j.intermet.2005.10.019

Xu, C. Z., Jiang, S. M., Bao, Z. B., Gong, J., and Sun, C. (2009). Isothermal Oxidation Behaviour of a Gradient NiCoCrAlSiY Coating Deposited by Arc Ion Plating on a Ni-Based Single crystal Superalloy. *Corrosion Sci.* 51, 1467–1474. doi:10.1016/j.corsci.2009.03.036

Yamaguchi, M., Inui, H., and Ito, K. (2000). High-temperature Structural Intermetallics. *Acta Materialia.* 48, 307–322. doi:10.1016/s1359-6454(99)00301-8

Zakeri, A., Bahmani, E., Sabour Rouh Aghdam, A., and Saeedi, B. (2020). A Comparative Study on the Microstructure Evolution of Conventional and Nanostructured MCrAlY Powders at High-Temperature. *Surf. Coat. Technol.* 389, 125629. doi:10.1016/j.surfcoat.2020.125629

Conflict of Interest: The authors declare that the research was conducted in the absence of any commercial or financial relationships that could be construed as a potential conflict of interest.

Publisher's Note: All claims expressed in this article are solely those of the authors and do not necessarily represent those of their affiliated organizations, or those of the publisher, the editors and the reviewers. Any product that may be evaluated in this article, or claim that may be made by its manufacturer, is not guaranteed or endorsed by the publisher.